RSC Publishing Biomaterials Science

Tailored intracellular delivery via a crystal phase transition in 400 nm vaterite particles

Journal:	*Biomaterials Science*
Manuscript ID:	Draft
Article Type:	Paper
Date Submitted by the Author:	n/a

Complete List of Authors:	Parakhonskiy, Bogdan; University of Trento, Italy, BIOtech research center, Department of Industrial Engineering; Shubnikov Institute of Crystallography, Foss, Cristina; University of Trento, Italy, BIOtech research center, Department of Industrial Engineering; INSTM-Consorzio Interuniversitario Nazionale per la Scienza e Tecnologia dei Materiali, Carletti, Eleonora; University of Trento, Italy, BIOtech research center, Department of Industrial Engineering; INSTM-Consorzio Interuniversitario Nazionale per la Scienza e Tecnologia dei Materiali, Fedel, Mariangela; University of Trento, Italy, ; University of Trento, Italy, BIOtech research center, Department of Industrial Engineering; INSTM-Consorzio Interuniversitario Nazionale per la Scienza e Tecnologia dei Materiali, Haase, Albrecht; University of Trento, Italy, Department of Physics Motta, Antonella; University of Trento, Italy, ; University of Trento, Italy, BIOtech research center, Department of Industrial Engineering; INSTM-Consorzio Interuniversitario Nazionale per la Scienza e Tecnologia dei Materiali, Migliaresi, Claudio; University of Trento, Italy, ; University of Trento, Italy, BIOtech research center, Department of Industrial Engineering; INSTM-Consorzio Interuniversitario Nazionale per la Scienza e Tecnologia dei Materiali, Antolini, Renzo; University of Trento, Italy, ; University of Trento, Italy, Department of Physics

Biomaterial Science Biomaterials Science Dynamic Article Links ►

Cite this: DOI: 10.1039/c0xx00000x

www.rsc.org/xxxxxx

PAPER

Tailored intracellular delivery via a crystal phase transition in 400 nm vaterite particles

Bogdan V. Parakhonsky[a,b*,^], Cristina Foss[a,c,^], Eleonora Carletti[a,c], Mariangela Fedel[a,c], Albrecht Haase[d], Antonella Motta[a,c], Claudio Migliaresi[a,c], and Renzo Antolini[d]

Received (in XXX, XXX) Xth XXXXXXXXX 20XX, Accepted Xth XXXXXXXXX 20XX
DOI: 10.1039/b000000x

Porous vaterite containers of 400 nm size are studied with respect to intracellular drug delivery applications. A generic crystal phase transition from vaterite to calcite serves as novel payload release mechanism, which reveals a delayed burst-release. This will permit control of the pharmacokinetics allowing for applications like preventive drug administration or scheduled application of pharmaceuticals during long term therapy. Experiments with two types of payloads, providing different molecular weights and zeta-potentials, demonstrate a flexible way of tailoring the payload delivery time *via* the molecular properties of the cargo. A dual *in-vitro* cellular uptake experiment with human ovarian carcinoma cells ES2 and human fibroblasts MRC5 shows no cytotoxicity, no influence on cell viability, and fast penetration of substance-loaded containers into cells. Flow cytometry proves high uptake rates and 3D microscopy analysis reveals the intracellular distribution.The abstract should be a single paragraph which summarises the content of the article.

1. Introduction

One of the main subjects of research in nanomedicine is the design of new carriers for drug delivery. Complex application schemes in diagnostics and therapy demand a high degree of control on a wide range of system properties [1]. Besides efficient substance loading, storage, and delivery to the targeted cells [2], also a well adjustable timing of the substance release has become a development objective [3]. High cost-effectiveness and biocompatibility complete the list of prerequisites for a successful carrier system [4]. Very promising regarding these criteria are porous inorganic nanoparticles [5,6]. They offer high chemical and mechanical stability, being at the same time extremely flexible in their structural parameters. This allows to create desired upload capacities and release rates for specific cargos [7]. Their hydrophilic character and the large surface and pore size allow the incorporation of a huge variety of payloads, extending e.g. over orders of magnitude in size [8,9]. The release properties can be varied from fast desorption to long retardation effects, creating local drug reservoirs [6,10,11]. Moreover, porous inorganic nanoparticles allow implementing release mechanisms which can be externally activated by various methods such as pH [12–14] or temperature [15,16] variation, ultrasound [17,18] or laser exposure [19–21]. Porous calcium carbonate in the form of polycrystalline vaterite spheres is one of the most promising systems in this respect [6,22]. For micrometer-sized vaterite capsules, many favorable properties have already been demonstrated, such as biocompatibility, high drug loading capacity, and payload protection [6,14,23,24]. However, only recently these capsules could successfully be scaled down to sub-micron sizes [25]. This implies an enormous increase of the system's potential for drug delivery applications [26,27,9] since the achieved mono-dispersed size distribution around 400 nm now allows to access to micrometer-sized cells or tissue.

After shrinking the size, an important issue is the investigation of the containers' release dynamics and its controllability. The two most common processes exploited for cargo release from porous particles are desorption-adsorption [6,10,11] and dissolution of the carriers [26]. But both processes offer rather limited control of the release rate [10]. However, realistic carrier systems for nanomedicine need control of the pharmacokinetics, two common scenarios are predisposed for controllable delayed substance release: preventive intake when direct administration is inconvenient e.g. for symptoms that follow circadian rhythms like hypertension, ischemic heart disease, asthma, or rheumatoid arthritis [28], the other is a scheduled application during long term therapy. e.g. of cancer [29], diabetes [30], ulcerative colitis [31], osteoporosis [32], or osteomyelitis [33].

In the carrier system based on vaterite proposed in this work, this temporal control can be realized by exploiting a novel feature of these particles in the sub-micron regime: the metastable carriers undergo a crystal phase transition from vaterite to calcite, during which the encapsulated substance is released almost completely. As recently shown, this mechanism allows a control of the payload delivery time *via* the properties of capsules and environment [25]. Within this paper first cellular uptake experiments of this sub-micron carriers are presented, their influence on cell vitality and metabolism is characterized, and a

flexible way of tailoring the substance release dynamics *via* the payload molecular structure is demonstrated.

2. Material and methods

2.1 Materials.

Sodium carbonate, calcium chloride, ethylene glycol, TRITC-dextran (m.w. 4400 Da), Rhodamine 6G, lactate dehydrogenase assay were purchased from Sigma-Aldrich-Fluka, alamarBlue assay, calcein AM, sodium pyruvate, phosphate buffered saline, non-essential amino acids, minimum essential medium were purchased from Invitrogen. RPMI-1640 medium, fetal bovine serum, streptomycin-penicillin, l-glutamine were purchased from Euroclone.

2.2. Vaterite preparation.

To prepare sub-micron vaterite spherical particles a standard protocol [25] was followed. Ethylene glycol (EG) was added to the reaction solution. Na_2CO_3 and $CaCl_2$ were dissolved each in 2 ml water and 10 ml EG. The $CaCl_2$/EG and Na_2CO_3/EG solutions were rapidly mixed with magnetic stirring for 3 h. When the process was finished, the $CaCO_3$ was dried for 1 h at 60°C.

2.3. Capsule characterization.

For surface and pore size analysis of the $CaCO_3$ sub-micron particles the BET method of N_2 adsorption-desorption was applied (TriStar, Micrometrics). The container morphology was measured with a field emission environmental scanning electron microscope (XL 30, Philips). The zeta-potential was measured using a particle size analyzer (Delsa, Beckman Coulter). Size distribution of the vaterite spheres and the transition between vaterite and calcite phase were imaged with magnifications from 5000× to 50000×. Statistical image analysis was performed using ImageJ (NIH) based on N=100 particles per sample.

2.4. Capsule loading.

After preparation, 7 mg of the vaterite containers were immersed in 1.5 ml of 0.01 mg/ml Rhodamine 6G (Rh6G) or 1 mg/ml TRITC-Dextran (TD4) water solutions at room temperature (RT) for 1 h for loading. The loaded capsules were washed 4 times by centrifugation, each time replacing the supernatant by water. The adsorption of the fluorescent probe was controlled by zeta-potential measurements using a particle size analyzer (Delsa, Beckman Coulter)

2.5. Spectrofluorometry.

The concentration of TD4 and Rh6G was measured in the supernatants *via* Spectrofluorometry (Cary Eclipse, Varian) to determine the amount of encapsulated molecules and the release dynamics. The fluorescence intensity detected at 520 nm and 550 nm allowed to measure the absolute concentration of Rh6G and TD4, respectively, using a calibration curve obtained from known concentrations. Unknown samples were diluted in water to ensure that measurements lie within the linear range of the calibration curve. Subtracting the concentration of molecules detected in the supernatant from those in the initial immersion solution gave the total amount of encapsulated molecules. To investigate the release process, loaded containers were resuspended in water or ethanol and allowed to incubate at RT in carefully sealed centrifuge tubes. After different times of incubation, the samples were centrifuged and the concentration of dye in the supernatant was measured.

2.6. Two-photon laser scanning microscopy.

The correlation between fluorescence intensity and particle phase was studied by two-photon laser scanning microscopy (2PM) (Ultima IV, Prairie Technologies) with a 100× objective (NA 1.0, water immersion, Olympus) and an ultra-short pulsed laser (Mai Tai Deep See HP, Spectra-Physics) as light source at 840 nm.

2.7. Cell preparation.

For the cell uptake experiments, human ovarian carcinoma cells ES2 were cultured in RPMI-1640 medium supplemented with 10% inactivated Fetal Bovine Serum (FBS), 1% streptomycin-penicillin, and 2 mM L-Glutamine until confluence. For the cytotoxicity and viability assays, cells were seeded in a 24-well plate at a density of 2×10^4 cells/cm^2 in 1.5 ml of medium and incubated at 37°C in a 5% CO_2 atmosphere. Human embryonic lung fibroblast cells MRC5 were cultured in Minimum Essential Medium (MEM) supplemented with 10% FBS, 1% streptomycin-penicillin, 2 mM L-Glutamine, 100 mM sodium pyruvate, and non-essential amino acids.

2.8. Cellular uptake experiments.

To study the uptake of vaterite containers, ES2 and MRC5 cells were seeded in Lab-Tek chamber slides (8 chambers, NUNC) at a density of 2×10^4 cells/cm^2 in 0.5 ml of medium and incubated at 37°C in a 5% CO_2 atmosphere.

For sterilization, empty and dye-loaded capsules were stored in pure ethanol at 4°C overnight, and then centrifuged at 3000 rpm for 4 min. The containers were subsequently suspended in sterile distilled water and centrifuged three times to remove the ethanol. Finally, containers were suspended in fresh medium at high (100 μg/ml) and low (30 μg/ml) concentration and used for cell incubation 24 h after seeding.

2.9. Cytotoxicity assay.

The cytotoxicity of carriers was analyzed by a lactate dehydrogenase assay (LDH). ES2 cells were seeded as previously described. First, cytotoxicity was evaluated in the case of direct contact of the vaterite containers with the cells at 100 μg/ml and 30 μg/ml. Cells cultured in complete medium without particles were employed as negative control. Second, to investigate the effects of the extracts, vaterite containers were left 72 h in a phosphate buffered saline (PBS) solution at 37°C at a concentration of 1 mg/ml. After incubation, the supernatant (extract) was collected and added to culture medium in an amount equal to 1/4 of the medium. This mixture substituted the culture medium in the 24-well plate after 24 h of culturing. In a negative control to the extracts, samples of fresh PBS were used. As positive control, 1 mM of Triton X-100 [34]- was added to the culture medium. After 24 h of incubation with extracts, containers, or control media, the LDH assay was conducted following the provider's instructions. The absorbance measured at 690 nm was subtracted from the absorbance at 492 nm to compensate for the sample turbidity. Statistical analysis was performed by one-way ANOVA on n = 3 independent samples. After Tukey's range test, significance was assigned at p-values

less than 0.05. Equality of variances was checked using the F-test with a significant level of 0.05.

2.10. Metabolic activity.

The cellular metabolic activity was measured using an alamarBlue assay according to manufacturer instructions. After 2, 4, 6, 8, 24, and 48 h of exposure to empty and dye-loaded spheres, ES2 cells were incubated for 3 h at 37°C in 1 ml of fresh culture medium with 10% of alamarBlue reagent. 1 ml of dye solution was incubated in empty wells as a control, its background fluorescence was subtracted from the signals of the seeded wells. Data was analysed using two-way ANOVA (n = 3) with assumption tests and parameters equivalent to the cytotoxicity analysis.

2.11. Confocal microscopy.

To visualize viable cells and evaluate vaterite container uptake a confocal laser microscopy system was used (Eclipse Ti-E, Nikon). After 2, 8, 24, and 48 h of incubation with Rh6G- and TD4-loaded vaterite spheres, cell layers were washed three times with fresh medium to remove free carriers and then stained with calcein AM. Cells were incubated with medium containing 0.1 mM of the reagent for 10 min at RT. All optical microscopy images were postprocessed using Matlab (Mathworks) and Amira (Visage imaging) performing fluorescence unmixing, linear interpolation, and image deconvolution.

2.12. Flow cytometry.

The cell uptake was quantitatively analyzed by flow cytometry for both cell types after 24 and 48 h of incubation. Cells were pelleted, fixed with formaldehyde solution (1% in PBS buffer) for 10 min at +4°C, centrifuged 10 min at 10000 rpm, resuspended in PBS at a concentration of 1 x 10^6 cells/ml, and transferred to 5ml tubes (BD Biosciences). Cell samples were then analyzed using a 4 colour flow cytometer FACSCalibur (Becton Dickinson). Forward and side scatter signals were analysed to identify cell populations. A background signal was obtained by measuring the autofluorescence of negative control samples containing unloaded cells. Cell samples with TD4-loaded particles were analyzed recording the signal in the FL-2 channel (ex. 488 nm, em. 585/42 nm), while the signal from Rh6G-loaded particles was recorded from the FL-1 channel (ex. 488 nm, em. 530/30 nm). Following instrumental optimization, the acquisition parameters (amplification and threshold) were kept constant throughout the whole experiment. For each sample 10,000 events were recorded. Data was analyzed with the CellQuest Pro 6.0 software (Becton Dickinson), providing median intensity values and percentage of stained cells above a 98-percentile threshold of the control sample fluorescence distribution. Differences in cell populations were analyzed with the Kolmogorov-Smirnoff test with a statistical significance of $p<=0.01$[35].

3. Results and discussion

3.1 Fabrication and loading of vaterite containers.

The particles were synthesized using the techniques described by Parakhonskiy et al. [25], their average size of 400 nm was determined from scanning electron microscopy (SEM) images. A Brunauer-Emmett-Teller (BET) analysis demonstrated that the obtained vaterite particles offer favorable morphological properties for substance encapsulation such as a surface of 22 m^2/g, an internal pore volume of 41%, and an average pore size of 35 nm. These material properties promise an excellent suitability of the vaterite capsules as efficient reservoir for substances in a wide range of molecular weights.

As proof-of-principle experiments, two fluorescent markers were encapsulated into the vaterite containers: Rhodamine 6G (Rh6G) with a low molecular weight of 480 Da and TRITC dextran (TD4) where the attachment of the dextran group increases the molecular weight by one order of magnitude to 4.4 kDa. In this way, payload uptake and release could be studied by fluorescence microscopy and spectrofluorometry for payloads of different molecular properties.

For the high molecular weight cargo TD4, the loading efficiency was 157(24) µg/mg. For the low molecular weight substance Rh6G, the loading efficiency depended on the number of washings. One to four repetitions resulted in efficiencies from 8(2) µg/mg to 7(2)*10^{-2} µg/mg. The surface properties of the loaded capsules were characterized by zeta-potential measurements. Particles with TD4 cargo maintained a negative zeta-potential (changing from -11 mV to -25 mV), while the capsules loaded with Rh6G changed to +4 mV.

3.2 Release mechanism.

Subsequently, substance release mechanisms were studied for the different weight cargos. The release dynamics was compared in three surrounding media, observing the loaded container fluorescence intensity together with the crystal phase by two-photon fluorescence microscopy (2PM) and the absolute concentration of the released molecules by spectrofluorometry. Fig. 1 demonstrates the results of these combined measurements. The initial state was pure vaterite containers confirmed by fluorescence and electron microscopy (Fig. 1A). The recrystallization process started when vaterite particles were immersed into a water-based solution: the single vaterite phase slowly turned into a mix of both phases, while after the completion of the recrystallization process only calcite crystals were observed (Fig. 1B). This process can be explained by the dissolution and ionization of the external layer of vaterite, seeding the formation of calcite crystals from the ions. Hence, the dissolution rate of vaterite controls the growth rate of calcite [36].

The fluorescence images demonstrate a release of the encapsulated dye during this recrystallization process, leaving the centers of the calcite monocrystals dark with residual dye attached only to their surfaces (Fig. 1B). The dye release curves are shown in Fig. 1C. In the case of capsules with the low molecular weight cargo Rh6G immersed in water, after day 1 and 2, 25(8)% of the encapsulated dye were found in the solution, which can be attributed to a desorption-adsorption process: the dye is slowly released until a dynamic equilibrium is obtained. After day 3 and 4, the recrystallization process speeded up the payload release, raising the amount of dye molecules in the solution to 40(7)%. After the complete recrystallization of all vaterite spheres at day 5, up to 86(13)% of the initially encapsulated dye was detected in the solution. The residual dye remained attached to the calcite surface or within inter-particle gaps.

Cite this: DOI: 10.1039/c0xx00000x

www.rsc.org/xxxxxx

PAPER

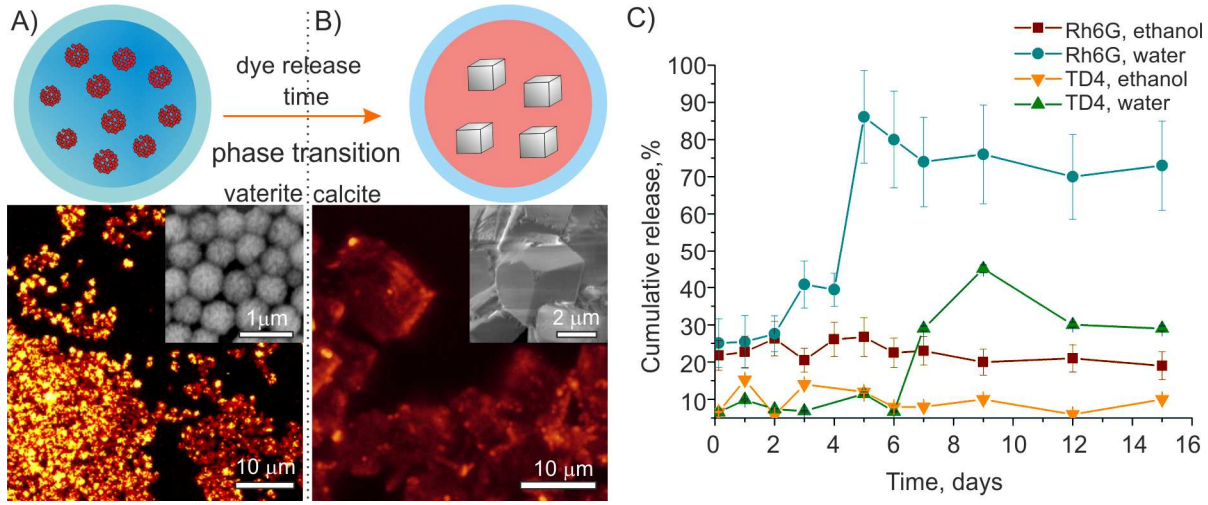

Figure 1. Capsules recrystallization in media: (A) and (B) represent a scheme of the release mechanism and the corresponding 2PM fluorescence images from the containers, with SEM images as insets. In (A) the carriers are in a pure vaterite phase with all dye encapsulated; (B) shows the calcite phase where the dye was released to the medium apart from residuals attached to the crystal edges; (C) shows dye release curves for different payloads measured by spectrofluorometry during the immersion in water and in ethanol.

A BET analysis during the phase transition from vaterite to calcite resulted in a particle surface shrinking from 22 to 6 m^2/g, owing to the transformation of porous spheres into rhombohedral monocrystals. The zeta-potential falls to 0 mV.

Immersion of the vaterite capsules in ethanol showed only a slow release *via* adsorption-desorption (Fig. 1C). The total amount of released dye was found to be 22(5)% at day 1 and did not increase significantly until day 6. This manifests a desorption-adsorption equilibrium without crystal phase transition. A negative zeta-potential measured throughout the whole experiment emphasizes the stability of the containers.

For the capsules loaded with the high molecular weight cargo TD4 instead, no recrystallization was observed in any of the media during the first week. During this time only a slow dye release (<10%) *via* desorption was measured (Fig. 1C). In this case the recrystallization process was completed only after 9 days. These dynamics can be explained by a strong attachment of TD4 to the vaterite surface, manifested also in the stronger negative zeta-potential, which prevents container aggregation by electrostatic repulsion. Moreover, polymers decrease the rate of dissolution, which consequently reduces the recrystallization and substance release rate with respect to lower weight cargos. These mechanisms open up the possibility to actively tune the release dynamics *via* the payload structure, such as the attachment of a dextran group to the fluorescent marker causing a retardation of the dye release.

3.3 Cytotoxicity and viability.

Before performing experiments on substance delivery to cultured cells, possible cytotoxic effects or influences on cell viability of the vaterite containers were tested. For this purpose, human ovarian carcinoma cells ES2 were incubated with Rh6G- and TD4-loaded capsules at two different concentrations to assess if there was a dependence on the amount of containers in contact with the cells or on the cargo type. Two strategies were employed to measure cytotoxicity: cells were put in direct contact with vaterite capsules suspended in culture medium or incubated with extracts (see Methods section). After 24 h of exposure, a lactate dehydrogenase (LDH)-based assay was performed. Results showed no significant differences in cell death between samples cultured at high and low concentrations of TD4- or Rh6G-loaded capsules and the corresponding negative control groups, i.e. cells with fresh culture medium (Fig. 2). No significant differences were also found between samples cultured with extracts and pure PBS. Instead, the absorbance measured for the positive control (cells cultured with 1 mM of cytotoxic Triton X-100) was significantly higher with respect to the absorbance detected for cells exposed to containers or their extracts. This proves that neither kind of vaterite containers are cytotoxic under any of the conditions tested.

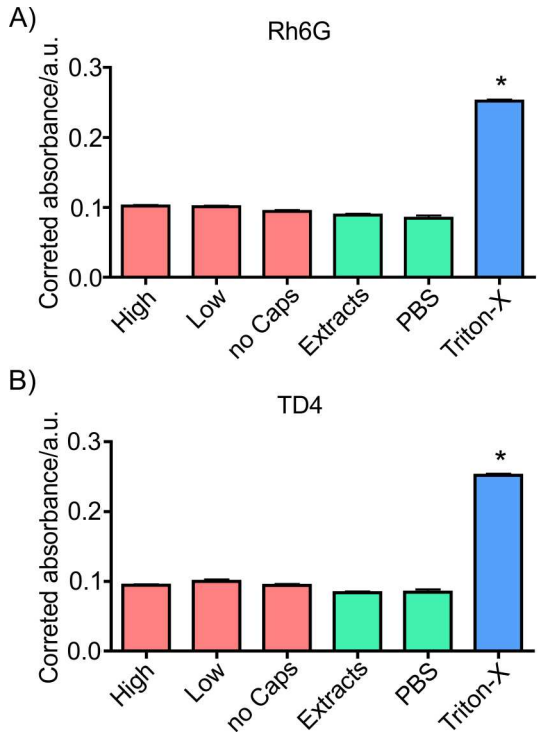

Figure 2. Cytotoxicity analysis of (A) Rh6G- and (B) TD4-loaded vaterite containers: the absorbance is proportional to the concentration of LDH, which in turn is directly dependent on cell death. ES2 cells were put in direct contact with vaterite capsules at two concentrations: 100 µg/ml (High) and 30 µg/ml (Low) for 24 h. Alternatively, extracts from containers were added to culture media (Extracts). Fresh medium (no Caps) and pure PBS were used as negative control. As positive control, cells were cultured in medium with 1 mM of Triton X-100. No significant differences could be detected between samples and negative control, while the absorbance of the positive control was significantly higher, indicating no cytotoxicity.

Then, cell viability was monitored for 48 h of incubation with both concentrations of dye-loaded capsules. The results are demonstrated in Fig. 3. The alamarBlue fluorescence signal is proportional to the number of viable cells in each sample at each time point. In all cultures, a significant increase in cell viability was found after 24 h and 48 h of incubation regardless of cargo type or concentration. The number of viable cells in the samples in contact with dye-loaded capsules at both concentrations showed no significant viability reduction with respect to the control samples without capsules, indicating that the presence of the vaterite containers did not modify cell metabolism or viability.

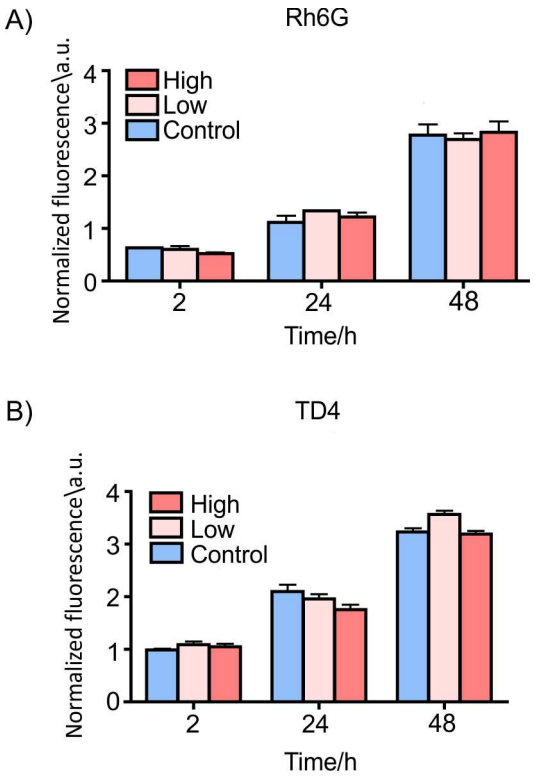

Figure 3. Cell viability measured at different times using an alamarBlue assay on ES2 cells incubated with 100 µg/ml (High) or 30 µg/ml (Low) of of (A) Rh6G- and (B) TD4-loaded vaterite containers in culture medium. Cells cultured without capsules were used as a control. The viability of cells in contact with containers shows no significant decrease with respect to the control samples at all times.

3.4 Cellular uptake.

An optical analysis of the uptake process was performed by confocal laser microscopy. Live cells were visualized using calcein AM (green channel in Fig. 4) and, simultaneously, the fluorescence distribution of the encapsulated payload was measured at different culture times (2, 4, 6, 8, 24, and 48 h) for both Rh6G and TD4 (for complete data see Figure S1). To assess if tumor and non-tumor cells exploited different uptake mechanisms or dynamics, the same analysis was performed on human MRC5 fibroblasts (Figure S2). The number of live cells increased with culture time, in accordance to the dynamics measured with the alamarBlue test.

Both cell lines ES2 and MRC5 showed very similar results: containers of different payloads reveal different uptake dynamics. For Rh6G-loaded containers, the fluorescence distributions demonstrate that the payload had entered the cells already after 2 h (Figures S1 and S2). The fluorescence signal from inside the cells increased significantly after 24 h and 48 h of incubation. This suggests a correlation between uptake mechanism and metabolic activity, since the number of metabolically active cells increased strongly at the same time points in the viability tests.

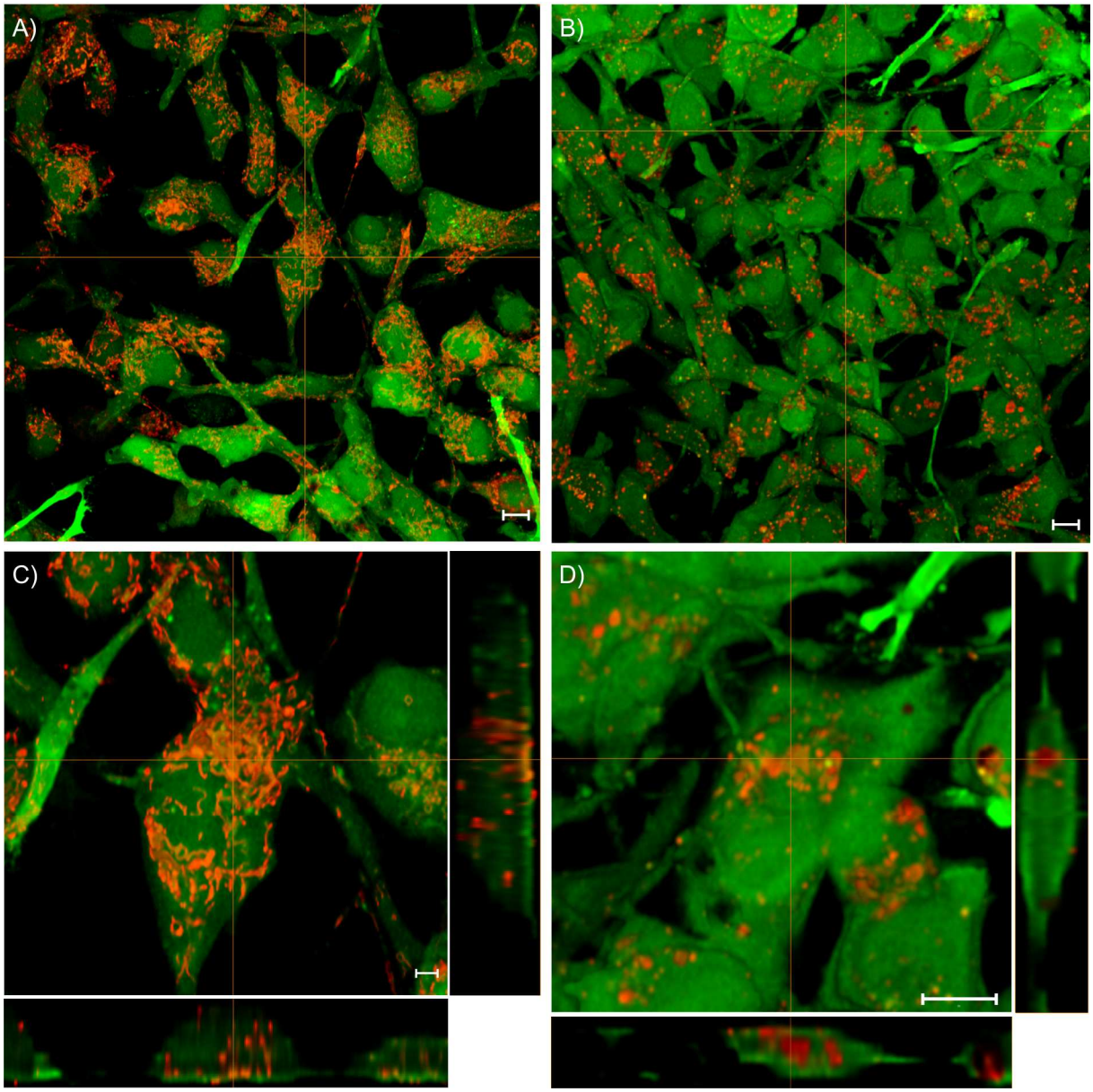

Figure 4. ES2 cells 48 h after adding the containers loaded with Rh6G (A, B) and TD4 (C, D). The green channel represents the calcein fluorescence labeling the cells, the red channel shows the fluorescent markers delivered by the containers The figures comprise projection views onto 3D image stacks(A, C) and a zoom onto single cells comprehended by perpendicular sections along the crosslines (B, D), which proves a complete internalization of the carriers. All scale bars correspond to 10 µm.

TD4-loaded containers instead, could not be detected within the cells after 2 h or 8 h and only with the increase of metabolic activity after 24 h, TD4 fluorescence inside the cells proved an uptake of the containers. This different uptake times can be explained again by the different payload properties: while loading the containers with TD4, their zeta-potential becomes more negative. Rh6G-loading instead, shifts the zeta-potential into the positive (see Paragraph 2.1) which favors the cellular uptake due to an attraction to the negatively charged cell membrane [37].

Fig. 4 shows ES2 cells after 48 h of incubation with dye-loaded containers. A complete internalization of the containers is proven by perpendicular image sections (Fig. 4 B,D) which complement the projection views onto the cell layers.

Also the fluorescence distribution within the cells turned out to be very different for the two payloads. Fig. 4 A and B show cells with Rh6G-loaded capsules, the dye is distributed within the cell in a form that suggests a partial release from the carriers and subsequent staining of the mitochondria [38,39]. The characteristic difference between the mitochondria morphology of fibroblasts and tumor cells is reflected by the fluorescence pattern showing rather elongated structures for the later [40,41]. This early release can be attributed to the desorption- adsorption process which was also observed in solution.

In the case of TD4-loaded containers instead (Figs. 4C, D), the shape and size of the fluorescent centers suggest that the dye is still confined in the vaterite spheres, which is in agreement with the release dynamics measurement in solution.

Cite this: DOI: 10.1039/c0xx00000x

www.rsc.org/xxxxxx

PAPER

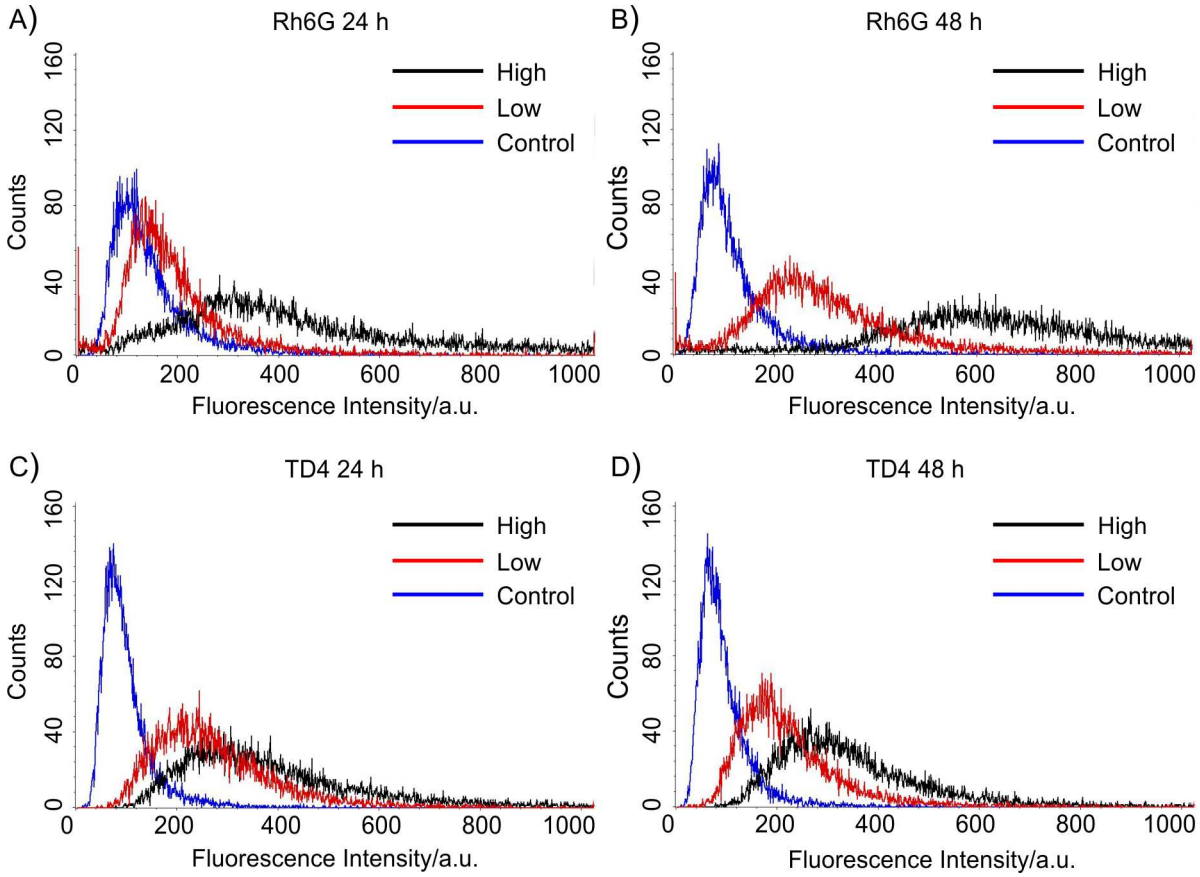

Figure. 5. Histograms of flow cytometry analysis of ES2 cells after 24h (A,C) and 48 h (B,D) of uptake. In (A,B) cells had been incubated with Rh6G-loaded containers, the black curves correspond to high container concentration, the red curve to low container concentration, and the blue curve to a control experiment without containers. Figures (C,D) show the same experiment for TD4-loaded containers. The significant shift in the fluorescence distributions manifests the efficient container uptake.

The cellular uptake of the containers was analyzed also quantitatively via flow cytometry. Fig. 5 shows the result for ES2 cells after 24 h and 48 h of incubation. The three curves correspond to cells incubated in medium with high concentration of containers, with low concentration, and without containers. The upper figures show data for Rh6G loaded containers, the lower figures for TD4-loaded containers. The corresponding results for the MRC5 cells can be found in the supplementary material (Figure S3).

A summary of the complete flow cytometry analysis is presented in Table 1. To discriminate the cell populations incubated with containers from the control cells without, a threshold was set at the 98%-percentile of the control sample histogram. The numbers in the table represent the percentage of cells above this threshold for the two cells types, the two container concentrations, and the two incubation times. For MRC5 cells, the uptake was significantly higher when incubated with high container concentration, compared to low concentration ($p<0.01$ according to the Kolmogorov-Smirnoff test applied to the selected histograms). Moreover, the uptake increases significantly from 24 to 48 h of incubation ($p<0.01$). The same increase with time and container concentration were observed for ES2 cells incubated with Rh6G-loaded containers ($p<0.01$).

When ES2 were cultured with TD4-loaded particles, uptake also increased significantly with suspended container concentrations. Instead, an inverse trend was observed regarding the dependence on incubation time. The percentage of cells above uptake-threshold decreased for both container concentrations ($p<0.01$), although at high concentration numbers were comparable (Table 1).

Cite this: DOI: 10.1039/c0xx00000x

www.rsc.org/xxxxxx

PAPER

Cell type	MRC5				ES2			
Container load	Rh6G		TD4		Rh6G		TD4	
Concentration	low	high	low	high	low	high	low	high
24 h uptake	6%	15%	30%	45%	6%	61%	49%	77%
48 h uptake	18%	38%	50%	80%	32%	98%	33%	77%

Table 1. Percentage of fluorescent cells above the 98%-percentile threshold of the control sample histogram without containers. These fractions demonstrate a significant uptake of fluorescent markers.

This may be due to the higher ES2 cells metabolism, possibly causing either an earlier release of containers by the cells or the disruption and detachment of TD4 molecules from the particles. This faster metabolic activity of ES2 cells is further confirmed by the generally higher percentage of cells above the uptake-threshold with respect to MRC5 cells under the same culture conditions. The fact that this shows up in TD4-loaded cells only, is another indication that dye release from the containers happens much faster for Rh6G- then for TD4- loaded containers, as observed in solution (Fig. 2), and it agrees with the observation from the confocal microscopy that Rh6G immediately stained the mitochondria, while TD4 remained confined within the containers after 24 hours (Fig. 4).

4. Conclusions

We characterized sub-micron vaterite containers for drug delivery applications obtaining very favorable results. Their substance loading capacity is high due to their porous structure. The crystal phase transition from vaterite to calcite exhibits a novel release mechanism, allowing a delayed burst-release of the cargo. The phase transition time and hence the release dynamics can be controlled by the molecular properties of the payload. This mechanism aims at drug delivery applications involving scheduled administration or time-consuming transport before reaching the release site, where it has clear advantages over common carrier systems which exhibit a burst release directly after suspension. Biocompatibility tests showed no indications of cytotoxicity and no influences on viability or metabolic activity. Cellular uptake experiments demonstrated fast penetration into the cells, Rh6G-loaded capsules released the dye into the cell, staining the mitochondria. In the TD4-loaded carriers an early release was avoided by adding a dextran group to the dye molecule. This increased crystal stability preventing recrystallization causing the dye to remain confined within the capsules inside the cells for at least 48 h.

Further studies are needed to fully characterize the crystal phase transition and the associated burst release directly within the cells. At the same time, the universality of vaterite containers can be exploited by implementing functional coatings allowing to actively trigger substance release by external controls such as temperature, ultrasound, or laser exposure.

Acknowledgment

We thank F. Piccoli, I. Caola (S. Chiara Hospital, Trento) and F. Tessarolo (BIOtech) for technical assistance with the SEM. B. Parakhonskiy. acknowledges funding by the Provincia Autonoma di Trento (Marie Curie Actions, Trentino COFUND).

Notes and references

a) BIOtech research center, Department of Industrial Engineering, University of Trento, via delle Regole 101, 38123 Mattarello, Italy Phone: +39 0461 882774; Fax: +39 0461 883659 e-mail address: bogdan.parakhonskiy@gmail.

b) Shubnikov Institute of Crystallography, Russian Academy of Science, Leninskii prospekt 59, Moscow 119333, Russia

c) INSTM-Consorzio Interuniversitario Nazionale per la Scienza e Tecnologia dei Materiali, via G. Giusti 9, 50121 Florence, Italy

d) Department of Physics, University of Trento, via Sommarive 14, 38123 Povo, Italy

^ These authors contributed equally.

† Electronic Supplementary Information (ESI) available: Images of ES2 and MRC5 cells at different culturing times after adding Rh6G- and TD4-loaded containers; Images visualizing mitochondria morphology differences between fibroblasts and tumor cells via staining with Rh6G-loaded containers; the FACS data for MRC5 cells.. See DOI: 10.1039/b000000x/

1. G. A. Hughes, *Nanomedicine*, 2005, **1**, 22–30.
2. H. Hillaireau and P. Couvreur, *Cell Mol. Life Sci.*, 2009, **66**, 2873–2896.
3. T. M. Allen and P. R. Cullis, *Science*, 2004, **303**, 1818–1822.
4. D. S. Kohane and R. Langer, *Chem. Sci.*, 2010, **1**, 441–446.
5. L. J. De Cock, S. De Koker, B. G. De Geest, J. Grooten, C. Vervaet, J. P. Remon, G. B. Sukhorukov, and M. N. Antipina, *Angew. Chem., Int. Ed. Engl.*, 2010, **49**, 6954–6973.
6. C. Peng, Q. Zhao, and C. Gao, *Colloids Surf., A*, 2010, **353**, 132–139.

7. M. Arruebo, *Wiley Interdiscip Rev.: Nanomed. Nanobiotechnol.*, 2011, **4**, 16–30.
8. S.-Y. Fu, X.-Q. Feng, B. Lauke, and Y.-W. Mai, *Composites, Part B*, 2008, **39**, 933–961.
9. M. P. Desai, V. Labhasetwar, G. L. Amidon, and R. J. Levy, *Pharm. Res.*, 1996, **13**, 1838–1845.
10. C. Washington, *Int. J. Pharm.*, 1990, **58**, 1–12.
11. Z. She, M. N. Antipina, J. Li, and G. B. Sukhorukov, *Biomacromolecules*, 2010, **11**, 1241–1247.
12. A. A. Antipov, G. B. Sukhorukov, S. Leporatti, I. L. Radtchenko, E. Donath, and H. Möhwald, *Colloids Surf., A*, 2002, **198-200**, 535–541.
13. G. B. Sukhorukov, A. Fery, and H. Möhwald, *Prog. Polym. Sci.*, 2005, **30**, 885–897.
14. D. V. Volodkin, R. von Klitzing, and H. Möhwald, *Angew. Chem., Int. Ed. Engl.*, 2010, **49**, 9258–9261.
15. K. Köhler, H. Möhwald, and G. B. Sukhorukov, *J. Phys. Chem. B*, 2006, **110**, 24002–24010.
16. K. Köhler, D. G. Shchukin, H. Möhwald, and G. B. Sukhorukov, *J. Phys. Chem. B*, 2005, **109**, 18250–18259.
17. H.-J. Kim, H. Matsuda, H. Zhou, and I. Honma, *Adv. Mater.*, 2006, **18**, 3083–3088.
18. A. M. Yashchenok, M. Delcea, K. Videnova, E. A. Jares-Erijman, T. M. Jovin, M. Konrad, H. Möhwald, and A. G. Skirtach, *Angew. Chem., Int. Ed. Engl.*, 2010, **49**, 8116–8120.
19. A. G. Skirtach, A. Muñoz Javier, O. Kreft, K. Köhler, A. Piera Alberola, H. Möhwald, W. J. Parak, and G. B. Sukhorukov, *Angew. Chem., Int. Ed. Engl.*, 2006, **45**, 4612–4617.
20. T. V. Bukreeva, B. V. Parakhonskiy, A. G. Skirtach, A. S. Susha, and G. B. Sukhorukov, *Crystallogr. Rep.*, 2006, **51**, 863–869.
21. A. G. Skirtach, P. Karageorgiev, M. F. Bédard, G. B. Sukhorukov, and H. Möhwald, *J. Am. Chem. Soc.*, 2008, **130**, 11572–11573.
22. Y. Wang, A. D. Price, and F. Caruso, *J. Mater. Chem.*, 2009, **19**, 6451–6464.
23. D. V. Volodkin, A. I. Petrov, M. Prevot, and G. B. Sukhorukov, *Langmuir*, 2004, **20**, 3398–3406.
24. G. B. Sukhorukov, D. V. Volodkin, A. M. Günther, A. I. Petrov, D. B. Shenoy, and H. Möhwald, *J. Mater. Chem.*, 2004, **14**, 2073–2081.
25. B. V. Parakhonskiy, A. Haase, and R. Antolini, *Angew. Chem., Int. Ed. Engl.*, 2012, **51**, 1195–1197.
26. J. Panyam and V. Labhasetwar, *Adv. Drug Delivery Rev.*, 2003, **55**, 329–347.
27. J. Rejman, V. Oberle, I. S. Zuhorn, and D. Hoekstra, *Biochem. J.*, 2004, **377**, 159–169.
28. M. Matsuo, *Int. J. Pharm.*, 1996, **138**, 225–235.
29. H. Okada, *Adv. Drug Deliv. Rev.*, 1997, **28**, 43–70.
30. X. M. Lam, E. T. Duenas, a L. Daugherty, N. Levin, and J. L. Cleland, *J. Control. Release*, 2000, **67**, 281–292.
31. P. Desreumaux and S. Ghosh, *Aliment. Pharmacol. Ther.*, 2006, **24 Suppl 1**, 2–9.
32. M. R. McClung, P. D. Miller, J. P. Brown, J. Zanchetta, M. a Bolognese, C. L. Benhamou, A. Balske, D. E. Burgio, J. Sarley, L. K. McCullough, and R. R. Recker, *Osteoporosis Int.*, 2012, **23**, 267–276.
33. I. Gürsel, F. Korkusuz, F. Türesin, N. G. Alaeddinoglu, and V. Hasirci, *Biomaterials*, 2001, **22**, 73–80.
34. J. Weyermann, D. Lochmann, and A. Zimmer, *Int. J. Pharm.*, 2005, **288**, 369–376.
35. I. T. Young, *J. Histochem. Cytochem.*, 1977, **25**, 935–941.
36. N. Spanos and P. G. Koutsoukos, *J. Cryst. Growth*, 1998, **191**, 783–790.
37. C. He, Y. Hu, L. Yin, C. Tang, and C. Yin, *Biomaterials*, 2010, **31**, 3657–3666.
38. L. V Johnson, M. L. Walsh, and L. B. Chen, *Proc. Natl. Acad. Sci. U. S. A.*, 1980, **77**, 990–994.
39. L. V. Johnson, M. L. Walsh, B. J. Bockus, and L. B. Chen, *J. Cell Biol.*, 1981, **88**, 526–535.
40. I. C. Summerhayes, T. J. Lampidis, S. D. Bernal, J. J. Nadakavukaren, K. K. Nadakavukaren, E. L. Shepherd, and L. B. Chen, *Proc. Natl. Acad. Sci. U. S. A.*, 1982, **79**, 5292–5296.
41. S. Goldstein and L. B. Korczack, *J. Cell Biol.*, 1981, **91**, 392–398.

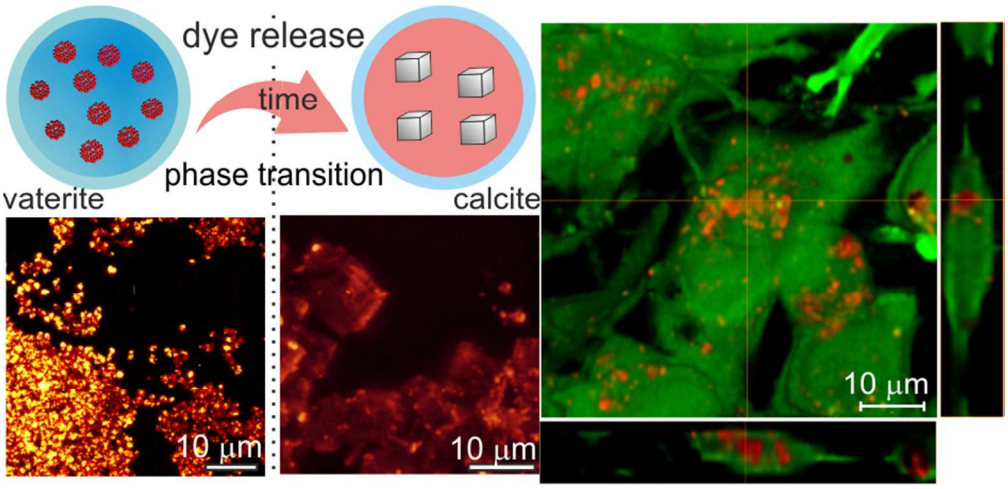

79x38mm (300 x 300 DPI)

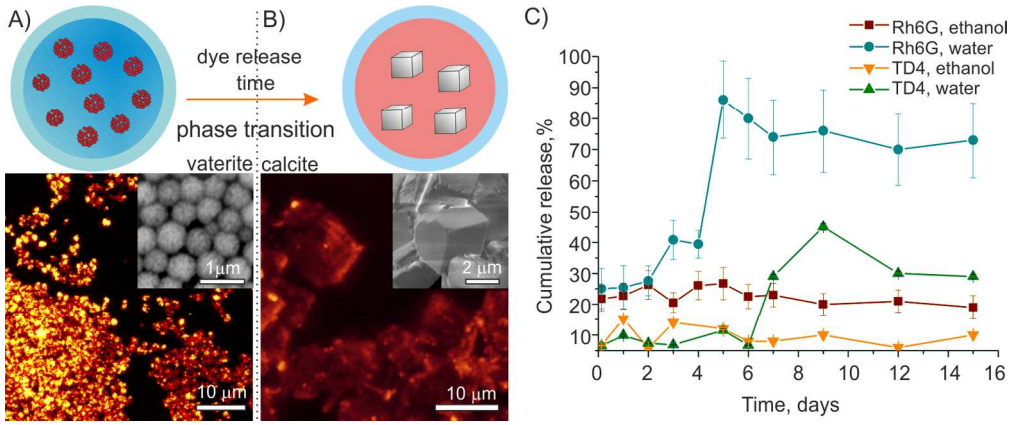

Figure 1. Capsules recrystallization in media: (A) and (B) represent a scheme of the release mechanism and the corresponding 2PM fluorescence images from the containers, with SEM images as insets. In (A) the carriers are in a pure vaterite phase with all dye encapsulated; (B) shows the calcite phase where the dye was released to the medium apart from residuals attached to the crystal edges; (C) shows dye release curves for different payloads measured by spectrofluorometry during the immersion in water and in ethanol.
157x65mm (300 x 300 DPI)

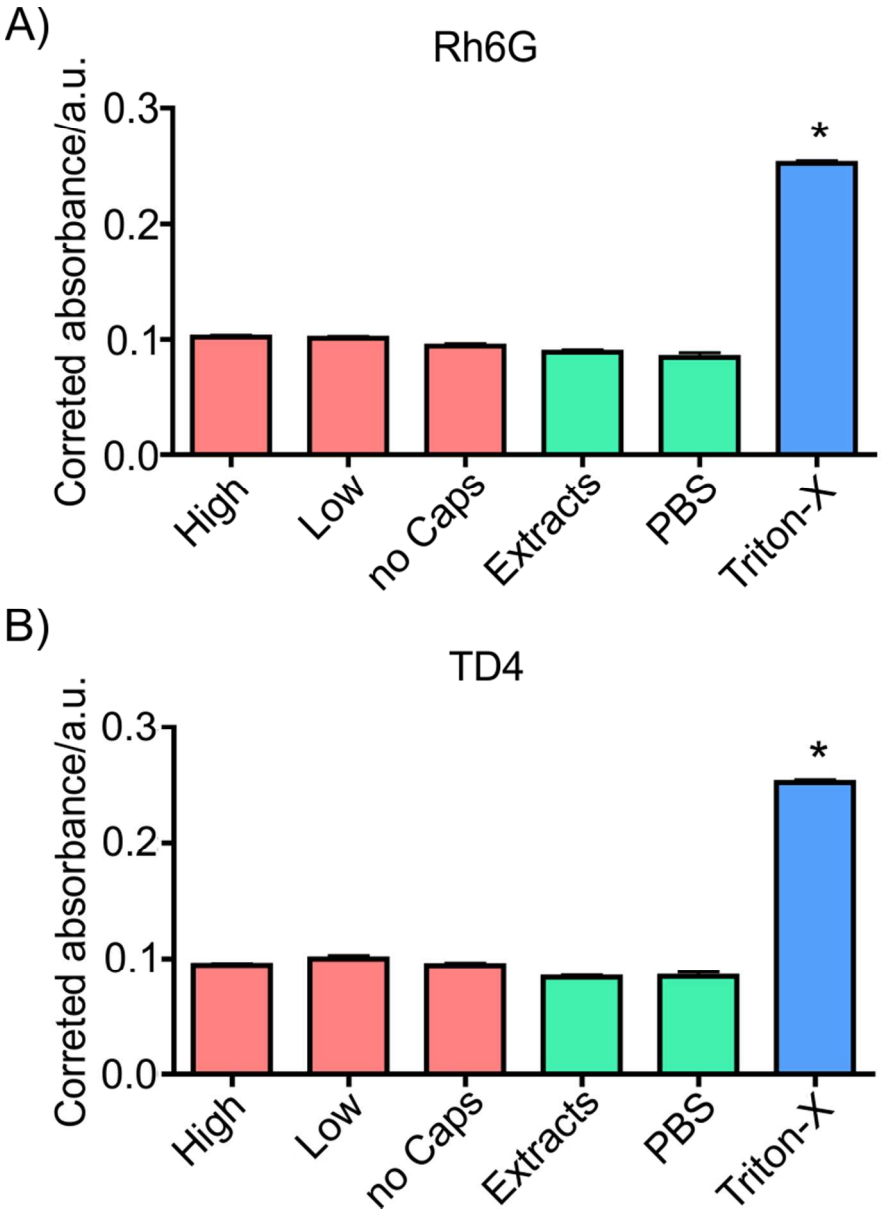

Figure 2. Cytotoxicity analysis of (A) Rh6G- and (B) TD4-loaded vaterite containers: the absorbance is proportional to the concentration of LDH, which in turn is directly dependent on cell death. ES2 cells were put in direct contact with vaterite capsules at two concentrations: 100 μg/ml (High) and 30 μg/ml (Low) for 24 h. Alternatively, extracts from containers were added to culture media (Extracts). Fresh medium (no Caps) and pure PBS were used as negative control. As positive control, cells were cultured in medium with 1 mM of Triton X-100. No significant differences could be detected between samples and negative control, while the absorbance of the positive control was significantly higher, indicating no cytotoxicity.
70x95mm (300 x 300 DPI)

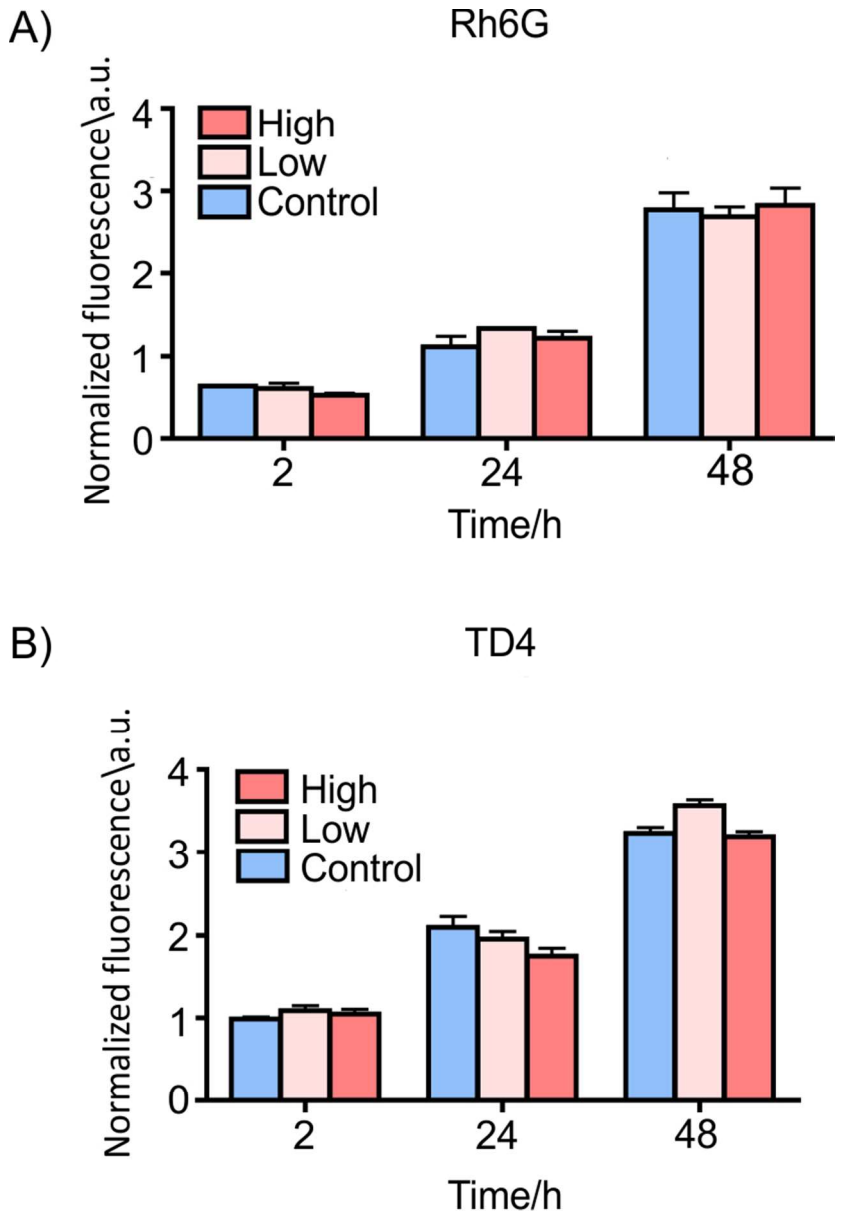

Figure 3. Cell viability measured at different times using an alamarBlue assay on ES2 cells incubated with 100 μg/ml (High) or 30 μg/ml (Low) of of (A) Rh6G- and (B) TD4-loaded vaterite containers in culture medium. Cells cultured without capsules were used as a control. The viability of cells in contact with containers shows no significant decrease with respect to the control samples at all times.
69x100mm (300 x 300 DPI)

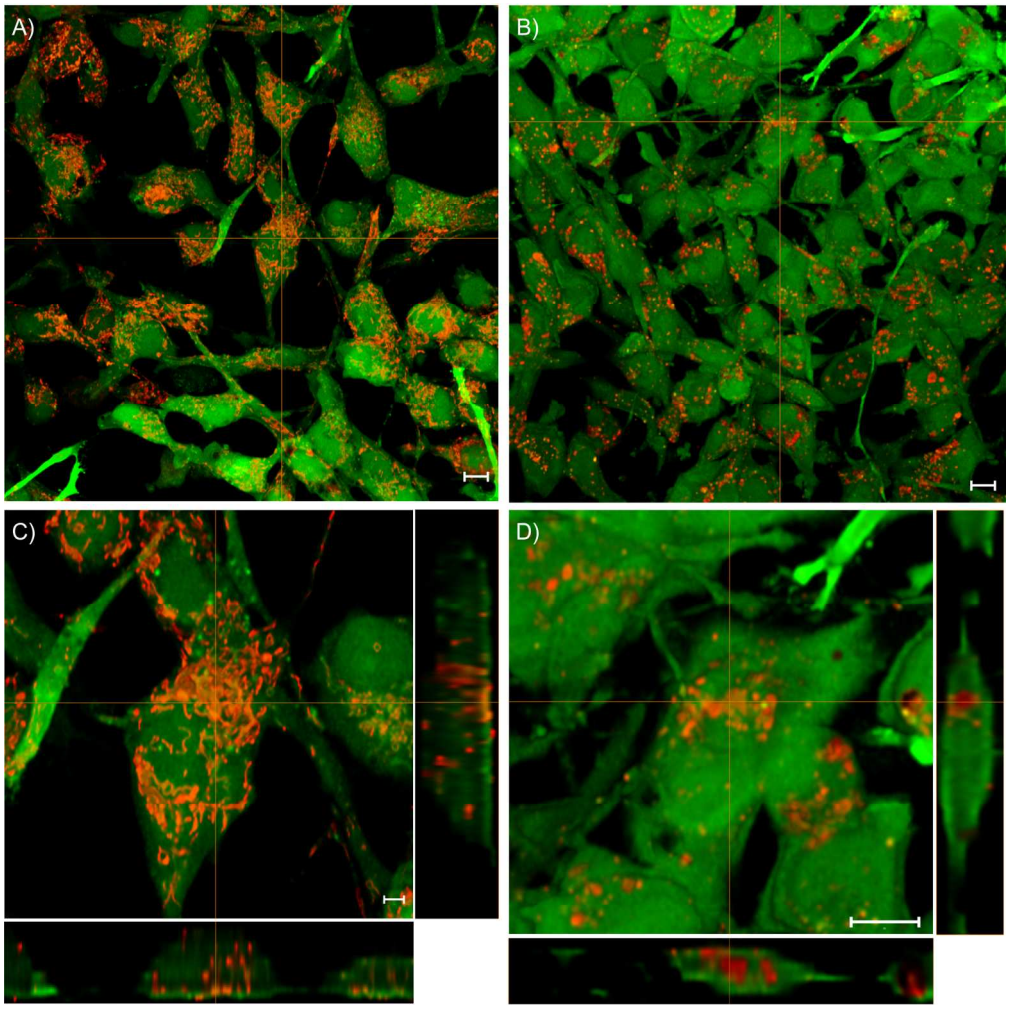

Figure 4. ES2 cells 48 h after adding the containers loaded with Rh6G (A, B) and TD4 (C, D). The green channel represents the calcein fluorescence labeling the cells, the red channel shows the fluorescent markers delivered by the containers The figures comprise projection views onto 3D image stacks(A, C) and a zoom onto single cells comprehended by perpendicular sections along the crosslines (B, D), which proves a complete internalization of the carriers. All scale bars correspond to 10 µm.
160x160mm (300 x 300 DPI)

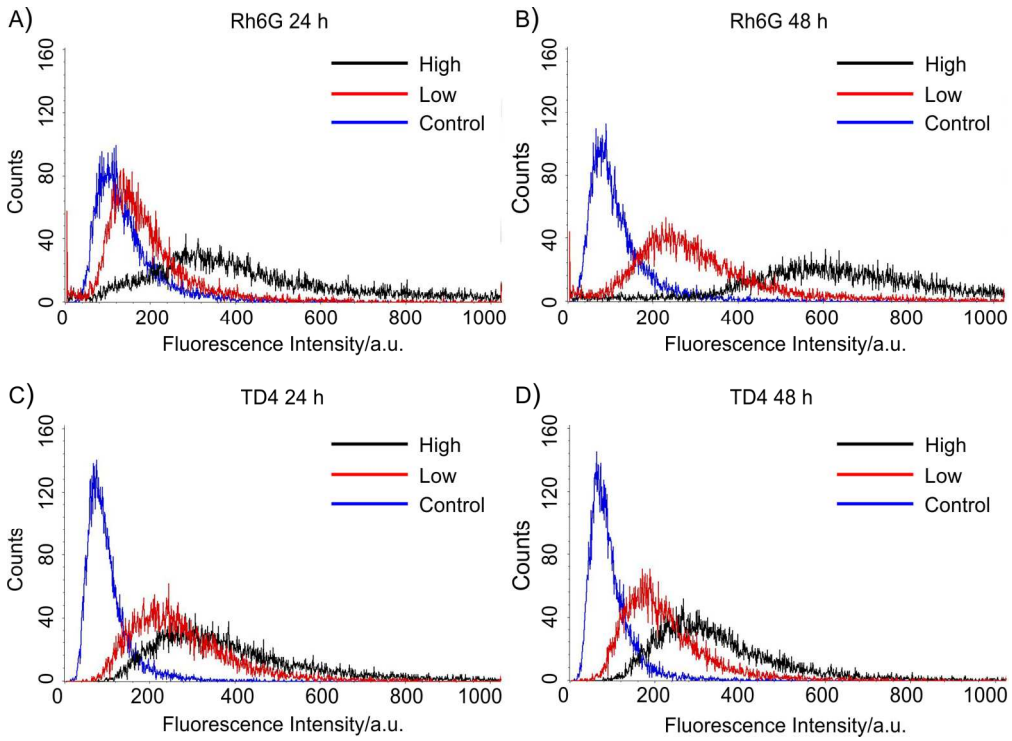

Figure. 5. Histograms of flow cytometry analysis of ES2 cells after 24h (A,C) and 48 h (B,D) of uptake. In (A,B) cells had been incubated with Rh6G-loaded containers, the black curves correspond to high container concentration, the red curve to low container concentration, and the blue curve to a control experiment without containers. Figures (C,D) show the same experiment for TD4-loaded containers. The significant shift in the fluorescence distributions manifests the efficient container uptake.
157x114mm (300 x 300 DPI)

Supplementary Information

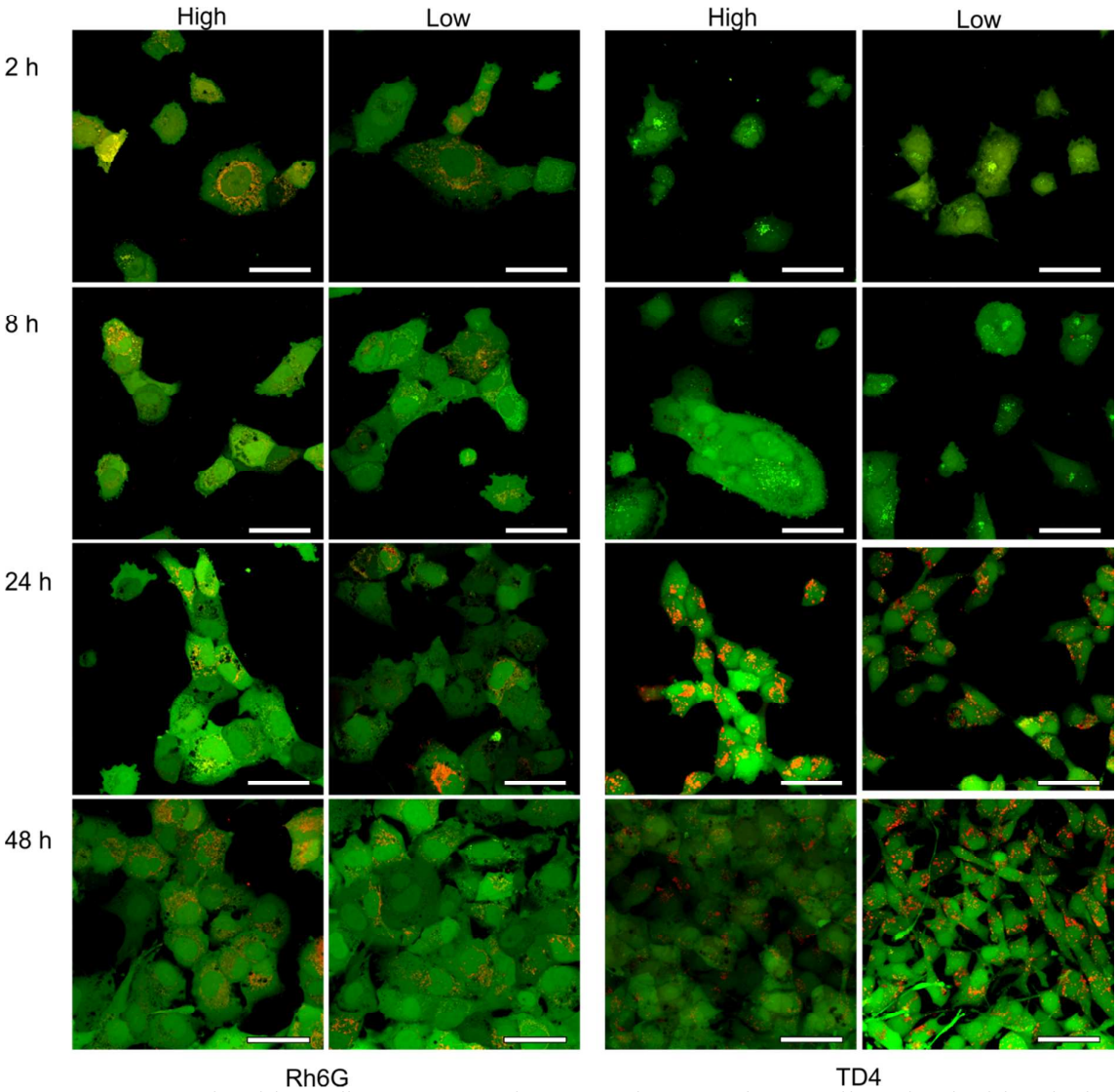

Figure S1a: Confocal laser fluorescence microscopy images of ES2 cells stained with calcein AM (green channel) after incubation with containers (red channel) loaded with Rh6G (left) and TD4 (right) at two different concentrations (high and low) at different culturing times (2, 8, 24, and 48 h) (scale bar 50 μm).

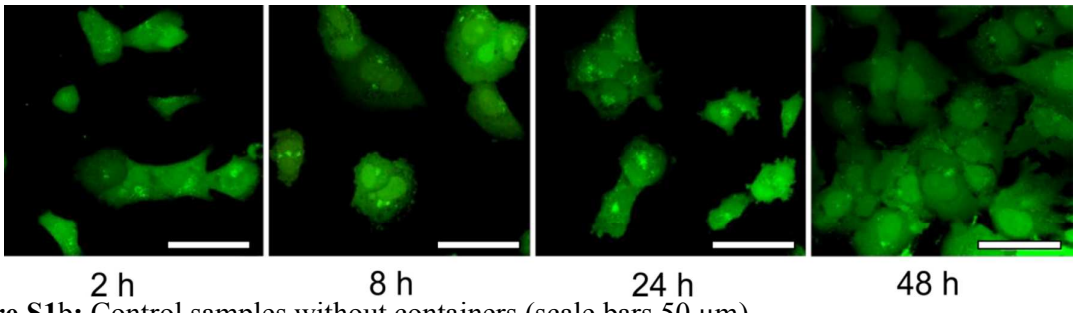

Figure S1b: Control samples without containers (scale bars 50 μm).

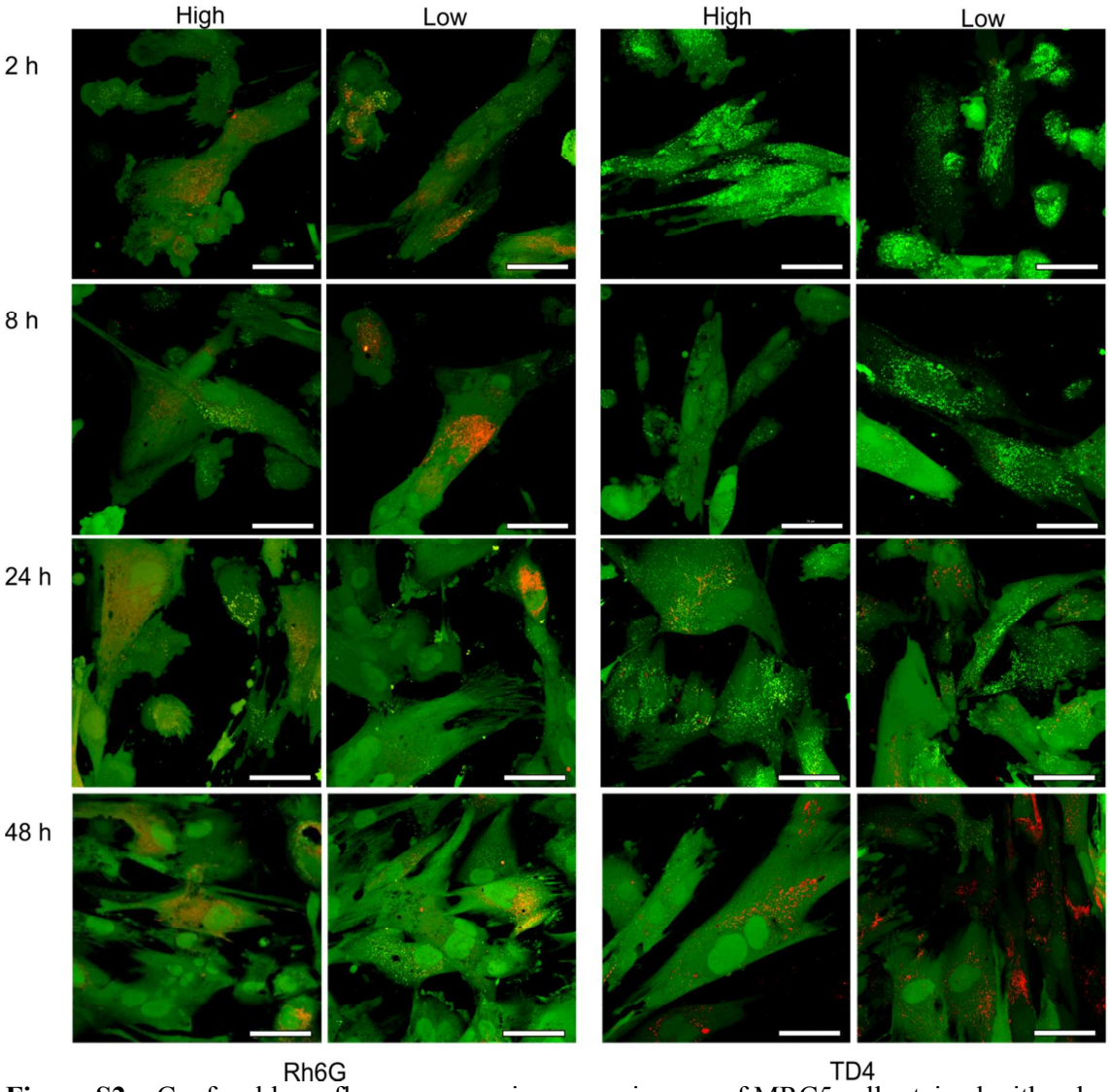

Figure S2a: Confocal laser fluorescence microscopy images of MRC5 cells stained with calcein AM (green channel) after incubation with containers (red channel) loaded with Rh6G (left) and TD4 (right) at two different concentrations (high and low) at different culturing times (2, 8, 24, and 48 h) (scale bars 50 µm).

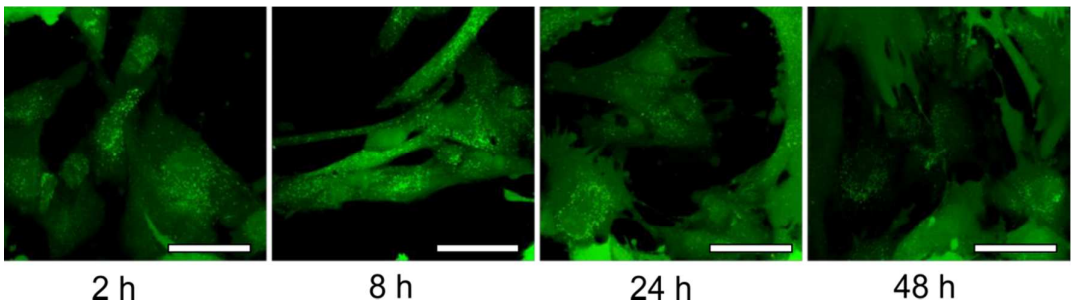

Figure S2b: Control images without containers (scale bars 50 µm).

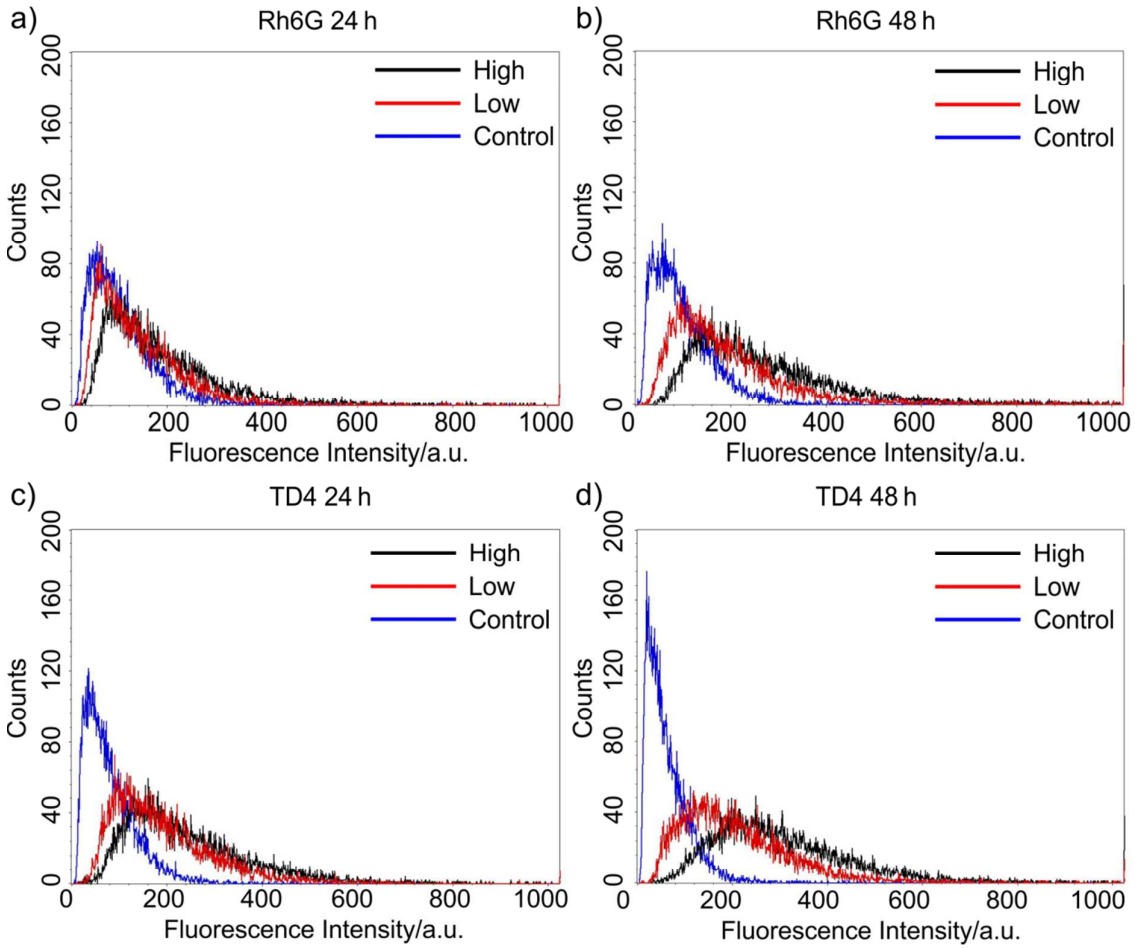

Figure S3: Histograms of flow cytometry analysis of MRC5 cells after 24h (a,c) and 48 h (b,d) of uptake. In (a,b) cells had been incubated in Rh6G-loaded containers medium, the black curves correspond to high container concentration, the red curve to low container concentration, and the blue curve to a control experiment without containers. Figures (c,d) show the same experiment for TD4-loaded containers.